Amplified 2-μm Thulium-Doped All-Fiber Mode-Locked Figure-Eight Laser

Charles W. Rudy, Karel E. Urbanek, Michel J. F. Digonnet, and Robert L. Byer

***Abstract*—We report the first mode-locked, thulium-doped fiber figure-eight laser. The mode-locked oscillator produces 1.5-ps pulses with 63 pJ of pulse energy at a 10.4-MHz repetition rate with a 3-nm bandwidth at a center wavelength of 2034 nm. After amplification, the pulses are compressed to 370 fs with ∼50 nJ of pulse energy. The oscillator can also operate in a square pulse regime, yielding stable pulses from ∼100 ps to 20 ns long with ∼100 nJ per pulse after amplification.**

***Index Terms*—Doped fiber amplifiers, fiber lasers, fiber nonlinear optics, optical pulses, optical solitons, ultrafast optics.**

I. Introduction

THULIUM-DOPED lasers have a wide gain spectrum ranging from 1.8 to 2.1 μm, depending on the host material. A pulsed source with this range of wavelengths has many uses, including dielectric laser-driven particle-acceleration [1], mid-IR generation for spectroscopy through either down-conversion [2] or supercontinuum generation [3], and eye-safer applications, such as remote sensing [4]. The broad gain spectrum makes Tm^{3+} an excellent candidate for generating extremely short mode-locked pulses that would satisfy the ultrafast operation requirement for the mentioned applications.

The well-known benefits of all-fiber mode-locked lasers include ease of alignment and compact packing, which limit external noise sources [5]. Tm-doped fiber lasers have previously been mode-locked using carbon nanotubes [6]–[8], SESAMs [9], nonlinear polarization rotation [10], and a combination of SESAM and a nonlinear amplifying loop mirror (NALM) [11], [12].

We developed an all-fiber mode-locked laser in the figure-eight laser (F8L) configuration, which consists of two coupled loops, as shown in Fig. 1. The loop on the left is a NALM [13], which acts as a fiber saturable absorber. The asymmetrically located gain medium causes the signals counter-propagating in the loop to accumulate different nonlinear phase shifts. At high power, this differential phase shift causes the signals to pass fully clockwise through the second loop. At low power, light is reflected by the NALM instead, i.e., transmitted counterclockwise into the second loop and blocked by the isolator [14].

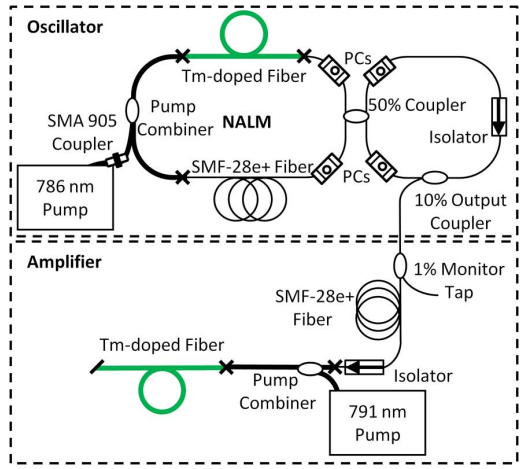

Fig. 1. Diagram of the figure-eight laser (oscillator) and amplifier. X denotes a splice between dissimilar fibers. The end of the gain fiber in the amplifier was angle-cleaved to prevent back reflections.

II. Experimental Design

Fiber components in the 2-μm wavelength range are still either unavailable commercially or exhibit modest performance, which limits options. A previous version of the F8L [15] used mainly C-band components as 2-μm components were largely unavailable. Many of the components have been replaced by 2-μm components; however, the new components have more loss than the C-band components at their respective operating wavelength range. The performance of Tm-doped fiber lasers will only improve as more 2-μm components are developed and the performance of current components increases.

The left loop of the F8L in Fig. 1 consisted of 7 m of SMF-28e+ fiber, 8 m of Nufern double-clad Tm-doped fiber with a 10-μm diameter core doped with 5 wt.% of Tm^{3+} and 130-μm octagonal cladding diameter, and assorted leads of SMF-28 fiber from the fiber components. SMF-28e+ fiber was chosen as the passive fiber because its measured loss at 2 μm is relatively low, namely around 10 dB/km, compared to $>$100 dB/km for the SMF-28 fiber. The gain fiber was cladding-pumped with a SMA 905 connectorized Dilas fiber-coupled laser diode at 786-nm through a $(2+1)\times 1$ pump combiner. The maximum usable pump power was limited to 9 W by the power rating of the pump combiner. The maximum pump power absorbed by the Tm-doped fiber was estimated to be 3 W.

The second loop, 3 m in length, consists of a 2-μm fiber-coupled isolator and a 10% fiber output coupler. The isolator had an insertion loss of 0.65 dB and an extinction ratio of 37 dB at 2 μm. A 50% 2×2 fused fiber coupler joined the two

Manuscript received February 01, 2013; revised March 27, 2013 and April 10, 2013; accepted April 13, 2013. Date of publication April 18, 2013; date of current version May 13, 2013. This work was supported in part by Joint Technologies Office Grant FA9550-10-1-0560, in part by the Department of Energy Grant FA9550-10-1-0227, and in part by the Department of Energy Grant DE-FG06-97ER41276.

The authors are with the Edward L. Ginzton Laboratory, Stanford University, Stanford, CA 94305 USA (e-mail: cwrudy@stanford.edu; kurbanek@stanford.edu; silurian@stanford.edu; rlbyer@stanford.edu).

Color versions of one or more of the figures in this paper are available online at http://ieeexplore.ieee.org.

Digital Object Identifier 10.1109/JLT.2013.2258891

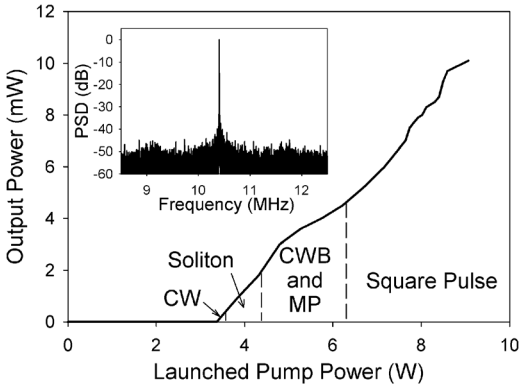

Fig. 2. The oscillator output power versus launched pump power is shown. At low pump power the F8L initially oscillates as a CW laser. As the launched pump power increases, the F8L then mode-locks and generates soliton pulses, the soliton pulses then began to experience CW breakthrough (CWB) and multi-pulsing (MP), and at ∼6 W of launched pump power, square pulses form. The inset shows the RF spectrum of the oscillator for the soliton pulse regime with a 300-Hz resolution bandwidth.

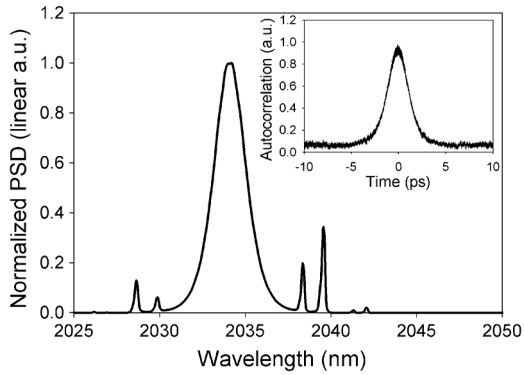

Fig. 3. The normalized oscillator power spectral density (PSD) and intensity autocorrelation (inset) are shown for the soliton pulse regime. The spectrum is centered around 2034 nm with a spectral bandwidth of 3 nm. In the inset, an autocorrelation trace width of 2.3 ps was measured, which corresponds to a pulse width of 1.5 ps.

loops together. The 2×2 central coupler had an insertion loss of 0.8 dB and its coupling ratio fluctuated around $50\% \pm 2\%$ over an 80 nm bandwidth centered at 2020 nm. The combined cavity length was ∼20 m. A polarization controller (PC) was inserted on each lead of the central coupler to ensure that the counter-propagating pulses interfered with maximum contrast.

The approximate round-trip loss of the F8L was 4 dB. Most of this loss originated from the passive fiber loss in the components made from SMF-28 fiber and from the insertion loss of these components, especially the isolator and central coupler. Also, the splices between the Tm-doped gain fiber and the passive fiber had a loss of 0.15 dB per splice, due to the difficulty of aligning an octagonal-clad fiber. As components in this wavelength range are developed commercially and mature, the losses will decrease and the laser performance will improve markedly.

The output of the F8L oscillator was passed through a 1% monitoring tap, an isolator (0.75 dB insertion loss and 37 dB isolation), and 13-m of SMF-28e+ to pre-chirp the pulse before entering the amplifier. The amplifier stage consisted of an 11-m length of the same gain fiber pumped with up to 7 W from a 791-nm Dilas fiber-coupled laser diode through a second $(2 + 1) \times 1$ pump combiner. This provided more than 20 dB of gain.

III. Oscillator Results

As the launched pump power was varied, as shown in Fig. 2, the F8L operated in several regimes. The oscillator initially operated as a continuous wave (CW) laser. As the pump power increased, CW oscillation became unstable and mode-locking self-started. At ∼4 W of pump power, the Tm-doped F8L generated pulses at a 10.4-MHz repetition rate with an average power of 0.66 mW, as measured by a thermal detector. This corresponds to an output pulse energy of 63 pJ. Fig. 3 shows the output spectrum, measured with a Yokogawa AQ6375 optical spectrum analyzer, of the soliton pulses, which had about a 3 nm bandwidth. An intensity autocorrelation trace of the 1.5 ps soliton pulses was measured using two photon absorption (TPA) in a Si photodiode and is shown in the inset of Fig. 3. Using the pulse width, 1.5 ps, and spectral bandwidth, 3 nm, the time-bandwidth product was calculated to be 0.33, which is nearly transform-limited.

Strong Kelly sidebands, which come from periodic spectral interference between the soliton wave and a co-propagating dispersive wave, were observed in the output spectrum. This is also a sign that the pulses were close to transform limited [16]. The Kelly sidebands contained 5% of the pulse energy. The separation of the sideband peaks from the main lobe was 4 nm [17].

The stability of the soliton operation strongly depended on and was quite sensitive to the position of the PCs. CW breakthrough would often occur (beginning with the Kelly sideband peaks) if the PCs were slightly shifted from the optimum positions for soliton operation. Since the central coupler had a coupling ratio that deviated from 50%, a CW path through the cavity existed. At low peak powers and with a central coupler deviation from 50% of ε, the NALM would reflect $4\varepsilon^2 T_{\rm OC}$, where $T_{\rm OC}$ is the transmission of the output coupler. For the measured 2% deviation in the central coupler, the reflectivity of the NALM would be -28 dB, which is not low enough to prevent CW oscillation. The PCs allowed for use of the coupler's polarization dependent loss (PDL) to compensate for this deviation from 50%, blocking the CW path. This partially explains the extreme sensitivity to PC positioning as well as the need to replace the 65% 2×2 coupler in [15].

The RF spectrum of the pulse train, shown in the inset of Fig. 2, was measured using a 10-GHz extended InGaAs photodiode and 40-GHz RF spectrum analyzer with a 300-Hz resolution bandwidth. From the RF spectrum, the amplitude noise was calculated to be 1.1% in the soliton mode-locking operation region [18]. Fabricating an all polarization-maintaining fiber F8L would increase the stability of the laser as well as reduce the effects of environmental fluctuations. To further increase the stability, the gain fiber can be core pumped by a stable 1.5-μm diode laser in combination with an erbium-doped fiber amplifier.

As the pump power increased, CW breakthrough and then multi-pulsing were observed. A type of multi-pulsing referred to as harmonic mode-locking, where the multiple pulses generated are temporally evenly separated, has also been observed with repetition rates of $>$100 MHz.

At ∼6 W, the F8L transitions to a new mode of operation where soliton pulses are no longer produced. As the peak power of the pulse reached the peak power allowed for maximum transmission through the NALM, the peak power of the pulse was clamped and further increase in gain produced a temporal

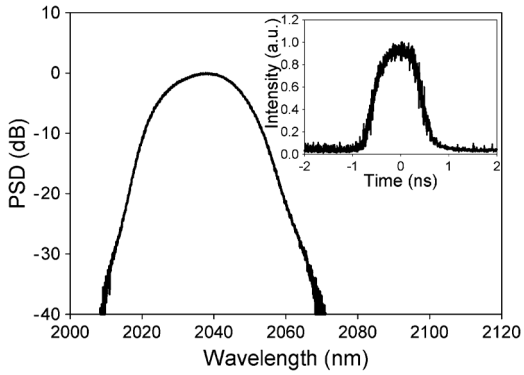

Fig. 4. The normalized PSD and temporal profile (inset) of the oscillator's square pulse regime are shown. Tuning of the pulse width (100 ps to 20 ns) and spectral width (15 nm to 25 nm) could be achieved by varying the pump power as well as the PCs. The spectral width shown is 20 nm, while the pulse width (inset) is 1 ns.

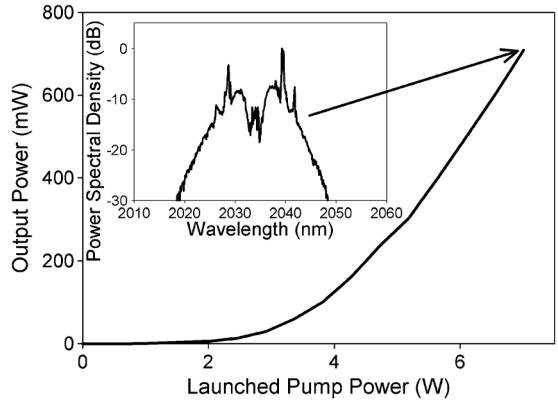

Fig. 5. The amplifier output power for varying launched pump power is shown for soliton input pulses. At $\sim$7 W of pump power, the amplifier output more than 700 mW of signal power. The normalized spectrum (inset) at the highest pump power is also depicted. The outer 3 dB bandwidth of the output pulse spectrum was over 12 nm.

and spectral broadening of the pulse [19]. This generated stable square-shaped pulses at a 10.4-MHz repetition rate with pulse widths from $\sim$100 ps to 20 ns and between 15 nm to 25 nm of spectral bandwidth, respectively. An example of the spectral and temporal characteristics of these pulses can be seen in Fig. 4, which shows a square pulse with a pulse width of 1 ns and bandwidth of 20 nm. Pulses from this regime may be useful for remote sensing (e.g. spectrally sensitive LIDAR [20]) and machining applications [21]. In addition to the pulse width variations introduced through modifying the pump power, the pulse width would change with cavity loss. The pulse width would change through adjusting of the position of the PCs, another indication of the PDL in the F8L.

The slope efficiency of the oscillator with respect to launched pump power is 0.2% (see Fig. 2). This low value was partially caused by poor coupling of the 786-nm fiber coupled diode pump into the pump combiner due to the use of an SMA 905 coupler with 100-μm core diameter fibers, causing $\sim$1.25 dB of loss. As a result of mismatch between the first cladding average diameter of the pump combiner (150 μm) and of the gain fiber (130 μm) the pumps experienced 0.5 dB of insertion loss in the pump combiner, as well as 0.15 dB of splice loss. In total, the 786-nm pump diode experienced $\sim$1.9 dB of loss before entering the gain fiber. High cavity loss, mainly from the 2-μm components, also reduces the efficiency. Again, this performance will only improve as the diversity and characteristics of commercial 2-μm fiber components progress in the future.

IV. Amplifier Results

Amplification of the oscillator has also been achieved. Fig. 5 shows the amplified output power for increasing launched pump power. The maximum slope efficiency of the amplifier was 22.7%. Spectral broadening and consequent temporal compression through self-phase modulation (SPM) in the amplifier [22] allowed for the slightly pre-chirped pulses to be compressed to 370 fs at the maximum average output power, 710 mW. The inset in Fig. 5 shows the output spectrum at the maximum pump power, with a bandwidth of just over 12 nm. The time-bandwidth product of the amplified soliton pulses was calculated to be 0.33. The Kelly sidebands were amplified more than the main lobe of the pulse, which became modulated due to SPM. The amplified Kelly sidebands contained less than 20% of the average power.

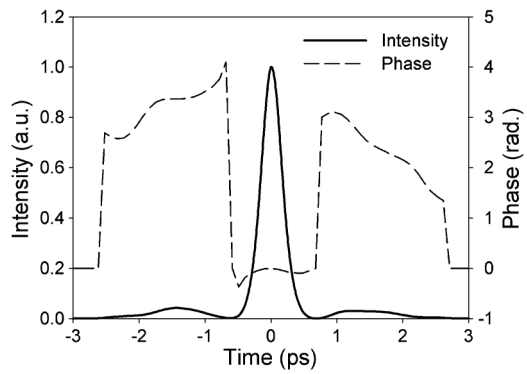

Fig. 6. The temporal reconstruction of the amplified pulse from the FROG measurement is shown for the maximum output power along with the estimated phase of the pulse. The reconstructed pulse width was 370 fs.

Fig. 6 shows the characterization of the amplified pulse performed with a SHG FROG system using a BBO crystal. The reconstructed pulse from the FROG measurement had a main lobe and two smaller sidelobes, which contain less than 15% of the pulse energy. The energy in the main lobe of the pulse was $\sim$50 nJ. The full width at half of maximum of the reconstructed pulse in the FROG measurement was 370 fs, more than a factor of 4 less than the oscillator's output pulse width. The peak power of the amplified pulse was then over 115 kW. The quadratic phase of the pre-chirped input pulse, which was introduced by the length of fiber between the oscillator and amplifier, was nearly compensated in the main lobe of the pulse through nonlinear chirp in the amplifier. This can be seen in the near-flat phase across the main lobe in Fig. 6.

In the oscillator's square pulse regime, amplification through the same amplifier yielded $\sim$1 W of average output power. The longer pulses with higher energy were able to extract more energy from the amplifier, with output energies of sim100 nJ, than in the case of the soliton pulses. To saturate the amplifier and extract more energy, a double pass configuration could be explored. Another possibility would be to split the amplifier into two stages.

V. Conclusion

In conclusion, we report the first Tm-doped all-fiber mode-locked F8L. Soliton pulses with 1.5 ps pulse width and 63 pJ of pulse energy were produced. After amplification, the pulses were compressed to a width of 370 fs with more than 12 nm of bandwidth around 2035 nm while achieving about 50 nJ of pulse energy. The oscillator could be tuned to produce square pulses of varying widths—from ∼100 ps to 20 ns, which were then amplified to pulse energies of ∼100 nJ. Including all modes of operation, the output pulse width of the fiber laser system can be varied to cover more than 4.5 orders of magnitude, from 370 fs to 20 ns.

References

[1] B. E. Carlsten, E. R. Colby, E. H. Esarey, M. Hogan, F. X. Kärtner, W. S. Graves, W. P. Leemans, T. Rao, J. B. Rosenzweig, C. B. Schroeder, D. Sutter, and W. E. White, "New source technologies and their impact on future light sources," *Nucl. Instr. Meth. Phys. Res. A*, vol. 622, pp. 657–668, 2010.

[2] N. Leindecker, A. Marandi, R. L. Byer, and K. L. Vodopyanov, "Broadband degenerate OPO for mid-infrared frequency comb generation," *Opt. Exp.*, vol. 19, no. 7, pp. 6296–6302.

[3] D. Buccoliero, H. Steffensen, O. Bang, H. Ebendorff-Heidepriem, and T. M. Monro, "Thulium pumped high power supercontinuum in loss-determined optimum lengths of tellurite photonic crystal fiber," *Appl. Phys. Lett.*, vol. 97, p. 061106, 2010.

[4] P. Kadwani, J. Chia, F. Altal, R. A. Sims, C. Willis, L. Shah, D. Killinger, and M. C. Richardson, "Atmospheric absorption spectroscopy using Tm:fiber sources around 2 microns," presented at the Atmospheric and Oceanic Propoagation of Electromagnetic Waves V, San Francisco, CA, USA, January 22, 2011, Paper 79240L.

[5] E. M. Dianov, "Fibre optics: Forty years later," *Quantum Electron.*, vol. 40, no. 1, pp. 1–6, 2010.

[6] M. A. Solodyankin, E. D. Obraztsova, A. S. Lobach, A. I. Chernov, A. V. Tausenev, V. I. Konov, and E. M. Dianov, "Mode-locked 1.93 μm thulium fiber laser with a carbon nanotube absorber," *Opt. Lett.*, vol. 33, no. 12, pp. 1336–1338, 2008.

[7] K. Kieu and F. W. Wise, "Soliton thulium-doped fiber laser with carbon nanotube saturable absorber," *IEEE Photon. Technol. Lett.*, vol. 21, pp. 128–130, 2009.

[8] R. A. Sims, P. Kadwani, T. S. McComb, C. C. Willis, L. Shah, and M. Richardson, "Fiber amplification of 2 μm picosecond pulses," presented at the CLEO QELS Conf., San Jose, CA, May 16–21, 2010, Paper CFK6.

[9] R. C. Sharp, D. E. Spock, N. Pan, and J. Elliot, "190-fs passively mode-locked thulium fiber laser with a low threshold," *Opt. Lett.*, vol. 21, no. 12, pp. 881–883, 1996.

[10] Q. Wang, T. Chen, and K. Chen, "Mode-locked ultrafast thulium fiber laser with all-fiber dispersion management," presented at the CLEO QELS Conf., San Jose, CA, USA, May 16–21, 2010, Paper CFK7.

[11] M. A. Chernyscheva, A. A. Krylov, P. G. Kryukov, and E. M. Dianov, "Nonlinear amplifying loop-mirror-based mode-locked thulium-doped fiber laser," *IEEE Photon. Technol. Lett.*, vol. 24, no. 14, pp. 1254–1256, Jul. 2012.

[12] M. A. Chernyscheva, A. A. Krylov, P. G. Kryukov, N. R. Arutyunyan, A. S. Pozharov, E. D. Obraztsova, and E. M. Dianov, "Thulium-doped mode-locked all-fiber laser based on NALM and carbon nanotube saturable absorber," *Opt. Exp.*, vol. 20, no. 26, pp. B124–B130, 2012.

[13] M. E. Fermann, F. Haberl, M. Hofer, and H. Hochreiter, "Nonlinear amplifying loop mirror," *Opt. Lett.*, vol. 15, no. 13, pp. 752–754, 1990.

[14] I. N. Duling, "All-fiber ring soliton laser mode locked with a nonlinear mirror," *Opt Lett.*, vol. 16, no. 8, pp. 539–541, 1991.

[15] C. W. Rudy, M. J. F. Digonnet, and R. L. Byer, "Thulium-doped germanosilicate mode-locked fiber lasers," presented at the FILAS Conf., San Diego, CA, Feb. 1, 2012, Paper FTh4A.

[16] S. M. J. Kelly, "Characteristic sideband instability of periodically amplified average soliton," *Electron. Lett.*, vol. 28, no. 8, pp. 806–807, 1992.

[17] J. N. Elgin and S. M. J. Kelly, "Spectral modulation and the growth of resonant modes associated with periodically amplified solitons," *Opt. Lett.*, vol. 18, no. 10, pp. 787–789, 1993.

[18] A. M. Weiner, *Ultrafast Optics*. New York, NY, USA: Wiley, 2009, pp. 139–144.

[19] D. J. Richardson, R. I. Laming, D. N. Payne, V. J. Matsas, and M. W. Phillips, "Pulse repetition rates in passive, femtosecond soliton fiber laser," *Electron. Lett.*, vol. 27, no. 16, pp. 1451–1453, 1991.

[20] B. J. Orr, *Infrared LIDAR Applications in Atmospheric Monitoring*. New York, NY, USA: Wiley, 2006.

[21] D. Gay, A. Cournoyer, P. Deladurantaye, M. Briand, V. Roy, B. Labranche, M. Levesque, and Y. Taillon, "Micro-milling process improvement using an agile pulse-shaping fiber laser," presented at the Photonics North, QC, Canada, May 24, 2009, Paper 73860R.

[22] K. J. Blow, N. J. Doran, and D. Wood, "Generation and stabilization of short soliton pulses in the amplified nonlinear Schrödinger equation," *J. Opt. Soc. Amer. B.*, vol. 5, pp. 381–390, 1988.

Charles W. Rudy is currently a doctoral candidate at Stanford University, Stanford, CA, in the group of Professor Robert Byer. He received the B.S.E. (2007) in electrical and computer engineering from the University of California, San Diego, La Jolla, CA, and the M.Sc. (2009) in electrical engineering from Stanford University.

He is currently a Research Assistant at Stanford University and has worked as a Research Assistant at the University of California, San Diego in the group of Professor Sadik Esener. In the past, he has worked with MEMS displays at Qualcomm in San Jose, CA, and ROADMs at Sumitomo Electric in Yokohama, Kanagawa, Japan. His current research interests include laser systems, fiber optics, nonlinear optics, telecommunications, and biophotonics.

Karel E. Urbanek received the B.S. in applied physics and the B.A. in economics from the University of California, Davis, CA, in 1997 and the M.Sc. in applied physics from Stanford University, Stanford, CA, in 2003. In 1996, he spent the summer working on rebuilding a COIL system at the National Science Institute, Prague, Czech Republic. He worked for Spectra-Physics first as a Technician and later an Engineering Technician from 1997 to 2000, gaining experience with gas, solid-state, and ultrafast lasers. Since 2003, he has been working as a Physical Sciences Research Assistant in the research groups of Professors Robert Byer and Martin Fejer in the Applied Physics department of Stanford University. Since 2010, he has also been working with the group of Professor Mark Schnitzer on laser dissection and imaging of drosophila melanogaster brains. His current interests include high-power fiber amplifiers, two-photon imaging, solid-state amplifiers, and nonlinear frequency conversion for use in near-infrared and visible laser systems.

Michel J. F. Digonnet received the degree of engineering from Ecole Supérieure de Physique et de Chimie de la Ville de Paris, the Diplome d'Etudes Approfondies in coherent optics from the University of Paris, Orsay, France (1978), and an MS (1980) and Ph.D. (1983) from the Department of Applied Physics at Stanford University, California. His doctoral research centered on WDM fiber couplers and single-crystal fiber lasers and amplifiers. He is a Research Professor in the Department of Applied Physics at Stanford University. His current interests include photonic-bandgap fibers and devices, slow and fast light in fibers, fiber optic gyroscopes, and fiber-based MEMS hydrophones and microphones. He has published about 250 articles, issued over 100 US patents, edited several scientific books, taught courses in fiber amplifiers, lasers, and sensors, and chaired numerous conferences on various aspects of photonics.

Robert L. Byer is the current President of The American Physical Society and has served as President of OSA and of IEEE LEOS. He has served as Vice Provost and Dean of Research at Stanford. He has been Chair of the Department of Applied Physics, Director of the Edward L. Ginzton Laboratory and Director of the Hansen Experimental Physics Laboratory. He is a founding member of the California Council on Science and Technology and served as Chair from 1995–1999. He was a member of the Air Force Scientific Advisory Board from 2002–2006 and has been a member of the National Ignition Facility since 2000.

Robert L. Byer has conducted research and taught classes in lasers and nonlinear optics at Stanford University since 1969. He has made extraordinary contributions to laser science and technology including the demonstration of the first tunable visible parametric oscillator, the development of the Q-switched unstable resonator Nd:YAG laser, remote sensing using tunable infrared sources and precision spectroscopy using Coherent Anti Stokes Raman Scattering (CARS).